Sensitivity studies for imaging a spherical object embedded in a spherically symmetric, two-layer turbid medium with photon-density waves

Yuqi Yao, Randall L. Barbour, Yao Wang, Harry L. Graber, and Jenghwa Chang

We present analytic expressions for the amplitude and phase of photon-density waves in strongly scattering, spherically symmetric, two-layer media containing a spherical object. This layered structure is a crude model of multilayered tissues whose absorption and scattering coefficients lie within a range reported in the literature for most tissue types. The embedded object simulates a pathology, such as a tumor. The normal-mode-series method is employed to solve the inhomogeneous Helmholtz equation in spherical coordinates, with suitable boundary conditions. By comparing the total field at points in the outer layer at a fixed distance from the origin when the object is present and when it is absent, we evaluate the potential sensitivity of an optical imaging system to inhomogeneities in absorption and scattering. For four types of background media with different absorption and scattering properties, we determine the modulation frequency that achieves an optimal compromise between signal-detection reliability and sensitivity to the presence of an object, the minimum detectable object radius, and the smallest detectable change in the absorption and scattering coefficients for a fixed object size. Our results indicate that (1) enhanced sensitivity to the object is achieved when the outer layer is more absorbing or scattering than the inner layer; (2) sensitivity to the object increases with the modulation frequency, except when the outer layer is the more absorbing; (3) amplitude measurements are proportionally more sensitive to a change in absorption, phase measurements are proportionally more sensitive to a change in scattering, and phase measurements exhibit a much greater capacity for distinguishing an absorption perturbation from a scattering perturbation.

1. Introduction

It has been shown that the propagation of light emitted from a sinusoidally varying intensity-modulated source in a strongly scattering medium is governed by the scalar Helmholtz wave equation. Such a wave is referred to as a photon-density wave (PDW)[1,2] or a diffuse photon-density wave (DPDW).[3] The mathematical analysis in the former instance starts from the diffusion approximation to the Boltzmann transport equation; the latter uses the diffusion equation. Here, we use the name PDW. An implication of these demonstrations is that light propagation can be analyzed in the frequency domain with theories and methodologies developed for electromagnetic (EM) and acoustic waves. The major difference between PDW and EM or acoustic waves is that wave number k of the PDW, which depends on the optical properties as well as on the modulation frequency, has a large imaginary part. Physically this implies an exponential attenuation of the wave's amplitude as the wave propagates away from the source, even for a nonabsorbing medium. Some important phenomena have been investigated, including the propagation of a PDW in an infinite multiple-scattering medium[4]; diffraction and reflection of a PDW from an absorbing or reflecting semi-infinite plane bounded by a straight edge and immersed in a uniform, infinite, strongly scattering medium[2]; refraction of a DPDW in piecewise homogeneous turbid media[3]; scattering of a DPDW by a spherical object immersed in an infinite, highly scattering medium[5]; and localization of a cylindrical

Y. Yao and Y. Wang are with the Department of Engineering, Polytechnic University, Brooklyn, New York 11201. R. L. Barbour is with the Department of Pathology and of Physiology and Biophysics, H. L. Graber is with the Department of Physiology and Biophysics, and J. Chang is with the Department of Pathology, State University of New York Health Science Center, Brooklyn, New York 11203.

Received 23 May 1995; revised manuscript received 12 September 1995.

0003-6935/96/040735-17$06.00/0

absorbing body by an interfering DPDW.[6] If near-infrared (NIR) intensity-modulated illumination is combined with frequency-resolved detection methods, imaging of the optical properties of a human hand[7] and inhomogeneous spherical objects embedded in a scattering media have been attempted.[8]

There are two general classes of problems regarding the interaction of PDW's with objects embedded in a strongly scattering medium. In a direct scattering problem (DSP), one computes the scattered field everywhere, given the source location and optical properties and geometry of the test medium. In an inverse scattering problem (ISP), the goal is to derive the properties of the test medium from the measured scattered field, usually from measurements made at the surface of the medium. It is the ISP that is of interest in clinical imaging. However, before one can quantitatively characterize an object by analysis of the scattered PDW, one must first solve the DSP for the given medium. This can be performed by computation of the numerical solutions to the transport or the diffusion equation. The solution of the diffusion equation is more tractable, especially when Monte Carlo methods are used to compute solutions to the transport equation. Analytic solutions to the diffusion equation are available for certain geometries, in particular the one considered here. We have adopted this approach to facilitate estimates of various practical experimental parameters, such as the required signal-to-noise ratio, the minimum detectable object size, and the absorption- and scattering-coefficient changes for a specified detector precision. In addition, one can also investigate the effects of varying the source and detector configurations to determine which are most sensitive to the presence of an object.

So far, most investigations of the DSP and ISP for PDW's have been limited to the case of an object embedded within an otherwise homogeneous, infinite medium. However, biological tissues are inhomogeneous media whose various components, such as skin, fat, and muscle, are typically arranged in layered structures.[9] In the present work, we study scattering from a spherical object embedded in the center of an infinite, two-layer spherically symmetric background medium. Figure 1 shows a sketch of the model medium that was examined. Depending on the values chosen, the optical thickness of the sphere varied from approximately 75 to 105 transport mean-free path lengths (tmfp) [1 tmpf = $1/(\mu_a + \mu_s')$]. Assuming a value of 1 mm for the tmfp of NIR light in tissue, this corresponds to a tissue thickness of approximately 7.5–10.5 cm. The geometry and dimensions chosen are intended to represent a crude model of multilayer tissue structures such as a breast or a head. For the latter, the outer layer would represent the skin and the underlying skull and the inner layer would correspond to the gray and the white matter, while the central object would simulate a pathology, such as a bleed in the ventricles. For other tissues, the outer layer can be viewed as overlying fat or muscle. Each layer is assigned optical properties within the ranges of most tissue types. The object is different from the surrounding layers in either its absorption or scattering coefficient. Here, we consider only the case of an object located at the center of the inner layer so that the test medium is in fact a spherically symmetric, three-layer medium.

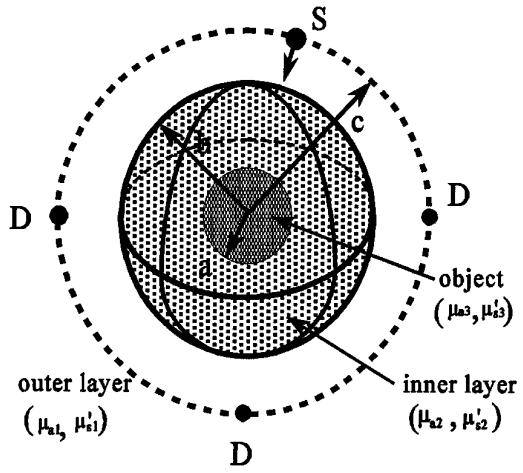

Fig. 1. Illustration of a spherical object embedded in a spherically symmetric, two-layer, highly scattering infinite medium, along with the source and detector configuration.

An analytic solution for the total field in this piecewise homogeneous structure, because of a source located on the surface of the outer layer, is derived by the use of the normal mode-series (NMS) method with appropriate boundary conditions. For a given set of background-medium properties, this solution is then used to derive the total field on the surface of the outer layer for various modulation frequencies, object sizes, and object properties. The objectives of this study are to determine (1) the modulation frequency that achieves an optimal compromise between signal detectability and sensitivity to the presence of an object, (2) the minimum detectable object radius for given properties of the object, (3) the smallest detectable change in the absorption coefficient for a given object radius, and (4) the smallest detectable change in the scattering coefficient for a given object radius. Four types of background media are examined: type I, in which the outer layer is more absorbing and both layers are equally scattering; type II, in which the outer layer is less absorbing and both layers are equally scattering; type III in which the outer layer is more scattering and both layers are equally absorbing; and type IV in which the outer layer is less scattering and both layers are equally absorbing. In addition to identifying limits on detectability, we report several new findings that may prove useful in evaluating methods for imaging dense scattering media.

In the following, we first derive the general solution for the total field for an arbitrary spherically

symmetric, three-layer, infinite medium. We then present results for the four types of background media described above.

2. Problem Formulation and Solution

We consider a spherical object embedded in a spherically symmetric, two-layer background medium. The geometry of this general three-layer structure is shown in Fig. 1. The radii of the object, the inner layer, and outer layer are denoted by a, b, and c, respectively. We adopt a spherical coordinate system with its origin at the center of the inner sphere. The absorption and scattering coefficients of the outer layer, the inner layer, and the object are denoted by μ_{a1} and μ'_{s1}, μ_{a2} and μ'_{s2}, and μ_{a3} and μ'_{s3}, respectively. The problem is to determine the total field at various points on the surface of the outer layer, $\mathbf{r} = (r, \theta, \phi)$, where $r = c$, that results from a sinusoidally varying, intensity-modulated point source of light placed at specific point, $\mathbf{r}' = (r', \theta', \phi')$, where $r' = c$ on the same surface.

For computational convenience, we neglect the boundary effect attributable to light exiting the medium across the external boundary and assume instead that the outer layer extends infinitely beyond the spherical surface where the source and detectors are located. Previous studies[5] that compared the solutions for finite and infinite media showed that the wave fronts in these two cases have similar shapes, except near the boundaries, and that the variations caused by an embedded object in the inner layer are unaffected by the boundaries of the outer layer. This is especially true when the detector is opposite the source in a transmission geometry.

Let $G(\mathbf{r}, \mathbf{r}')$ represent the photon density at $\mathbf{r}$ that is due to a unit-strength point source at $\mathbf{r}'$. Then $G(\mathbf{r}, \mathbf{r}')$ is the Green's function for the following nonhomogeneous Helmholtz wave equation[2,10,11]:

$$\nabla^2 G_j(\mathbf{r}, \mathbf{r}') + k_j^2 G_j(\mathbf{r}, \mathbf{r}') = -\delta(\mathbf{r} - \mathbf{r}'), \quad \text{for } \mathbf{r} \in \Omega_j, \qquad j = 1, 2, 3. \tag{1}$$

In Eq. (1), Ω_1 refers to $r \geq b$ (i.e., the outer layer), Ω_2 to $a \leq r < b$ (i.e., the inner layer), and Ω_3 to $0 \leq r < a$ (i.e., the object). The squared complex wave number is given by

$$k_j^2 = -\frac{\mu_{aj}}{D_j} + i\,\frac{\omega}{v_j D_j}, \tag{2}$$

with $\omega = 0$ for dc and $\omega \neq 0$ for ac and where v_j is the speed of a photon in Ω_j, $D_j = 1/3(\mu_{aj} + \mu'_{sj})$ is the diffusion coefficient, and μ_{aj} and μ'_{sj} are the absorption and scattering coefficients, respectively, in Ω_j. The wave number is, in general, complex and is denoted by $k_j = \beta_j + i\alpha_j$, where the attenuation factor α_j and the phase factor β_j are, respectively,

$$\alpha_j = \sqrt{\mu_{a_j}/2D_j}\,[1 + (\omega/v\mu_{a_j})^2 + 1]^{1/2},$$
$$\beta_j = \sqrt{\mu_{a_j}/2D_j}\,[1 + (\omega/v\mu_{a_j})^2 - 1]^{1/2}, \tag{3}$$

The Green's function G is subject to the following boundary conditions[12,13]:

(1) The photon density G is continuous at $r = b$ and $r = a$:

$$G_2|_{r=b} = G_1|_{r=b}, \qquad G_3|_{r=a} = G_2|_{r=a}. \tag{4}$$

(2) The photon current $\mathbf{J}$ is continuous at $r = b$ and $r = a$:

$$\mathbf{r} \cdot \mathbf{J}_2|_{r=b} = \mathbf{r} \cdot \mathbf{J}_1|_{r=b}, \qquad \mathbf{r} \cdot \mathbf{J}_3|_{r=a} = \mathbf{r} \cdot \mathbf{J}_2|_{r=a}. \tag{5}$$

(3) G is bounded at $r = 0$ and satisfies a radiation condition at $r \to \infty$.

The total field in the outer layer can, in general, be interpreted as a superposition of the incident spherical wave G_i and a scattered spherical wave G_{s1}, i.e.,

$$G_1(\mathbf{r}, \mathbf{r}') = G_i(\mathbf{r}, \mathbf{r}') + G_{s1}(\mathbf{r}, \mathbf{r}'), \qquad r > b. \tag{6}$$

Similarly, the total field in the inner layer can be represented as the sum of a transmitted spherical wave G_{t1} and a scattered field G_{s2}:

$$G_2(\mathbf{r}, \mathbf{r}') = G_{t2}(\mathbf{r}, \mathbf{r}') + G_{s2}(\mathbf{r}, \mathbf{r}'), \qquad a < r < b. \tag{7}$$

The total field in the object consists of a transmitted spherical wave G_{t3}:

$$G_3(\mathbf{r}, \mathbf{r}') = G_{t3}(\mathbf{r}, \mathbf{r}'), \qquad r < a. \tag{8}$$

Each of the five waves in Eqs. (4)–(8) can be expanded into a series of Legendre functions and spherical Bessel functions,[14,15] as follows:

(1) Outer layer:

$$G_i(\mathbf{r}, \mathbf{r}') = \left[\frac{ik_1}{4\pi} \sum_{n=0}^{\infty} \sum_{m=0}^{n} (2 - \delta_m)(2n + 1)\,\frac{(n - m)!}{(n + m)!}\right] \cdot [h_n^{(1)}(k_1 r')\, j_n(k_1 r) P_n^m(\cos\theta) P_n^m(\cos\theta') \times \cos m(\phi - \phi')], \tag{9}$$

$$G_{s1}(\mathbf{r}, \mathbf{r}') = \left[\frac{ik_1}{4\pi} \sum_{n=0}^{\infty} \sum_{m=0}^{n} A_{mn}(2 - \delta_m)(2n + 1)\,\frac{(n - m)!}{(n + m)!}\right] \cdot [h_n^{(1)}(k_1 r') h_n^{(1)}(k_1 r) P_n^m(\cos\theta) P_n^m(\cos\theta') \times \cos m(\phi - \phi')]. \tag{10}$$

Table 1. Optical Properties of Background-Media Types I–IV

Medium	Outer Layer μ_a (cm^{-1})	Outer Layer μ_s' (cm^{-1})	Inner Layer μ_a (cm^{-1})	Inner Layer μ_s' (cm^{-1})	Diameter (tmfp)
Type I	0.08	10.0	0.04	10.0	80
Type II	0.02	10.0	0.04	10.0	80
Type III	0.04	20.0	0.04	10.0	105
Type IV	0.04	5.0	0.04	10.0	75

(2) Inner layer:

$$G_{t2}(\mathbf{r},\mathbf{r}') = \left[\frac{ik_1}{4\pi}\sum_{n=0}^{\infty}\sum_{m=0}^{n} B_{mn}(2-\delta_m)(2n+1)\frac{(n-m)!}{(n+m)!}\right] \cdot [h_n^{(1)}(k_1 r')\, j_n(k_2 r) P_n^m(\cos\theta) P_n^m(\cos\theta') \times \cos m(\phi-\phi')], \quad (11)$$

$$G_{s2}(\mathbf{r},\mathbf{r}') = \left[\frac{ik_1}{4\pi}\sum_{n=0}^{\infty}\sum_{m=0}^{n} C_{mn}(2-\delta_m)(2n+1)\frac{(n-m)!}{(n+m)!}\right] \cdot [h_n^{(1)}(k_1 r')\, y_n(k_2 r) P_n^m(\cos\theta) P_n^m(\cos\theta') \times \cos m(\phi-\phi')]. \quad (12)$$

(3) Object:

$$G_{t3}(\mathbf{r},\mathbf{r}') = \left[\frac{ik_1}{4\pi}\sum_{n=0}^{\infty}\sum_{m=0}^{n} D_{mn}(2-\delta_m)(2n+1)\frac{(n-m)!}{(n+m)!}\right] \cdot [h_n^{(1)}(k_1 r')\, j_n(k_3 r) P_n^m(\cos\theta) P_n^m(\cos\theta') \times \cos m(\phi-\phi')]. \quad (13)$$

In Eqs. (9)–(13), A_{mn}, B_{mn}, C_{mn}, and D_{mn} are the unknown expansion coefficients; j_n, y_n, and $h_n^{(1)}$ are the spherical Bessel function, the spherical Neuman function, and the spherical Hankel function of the

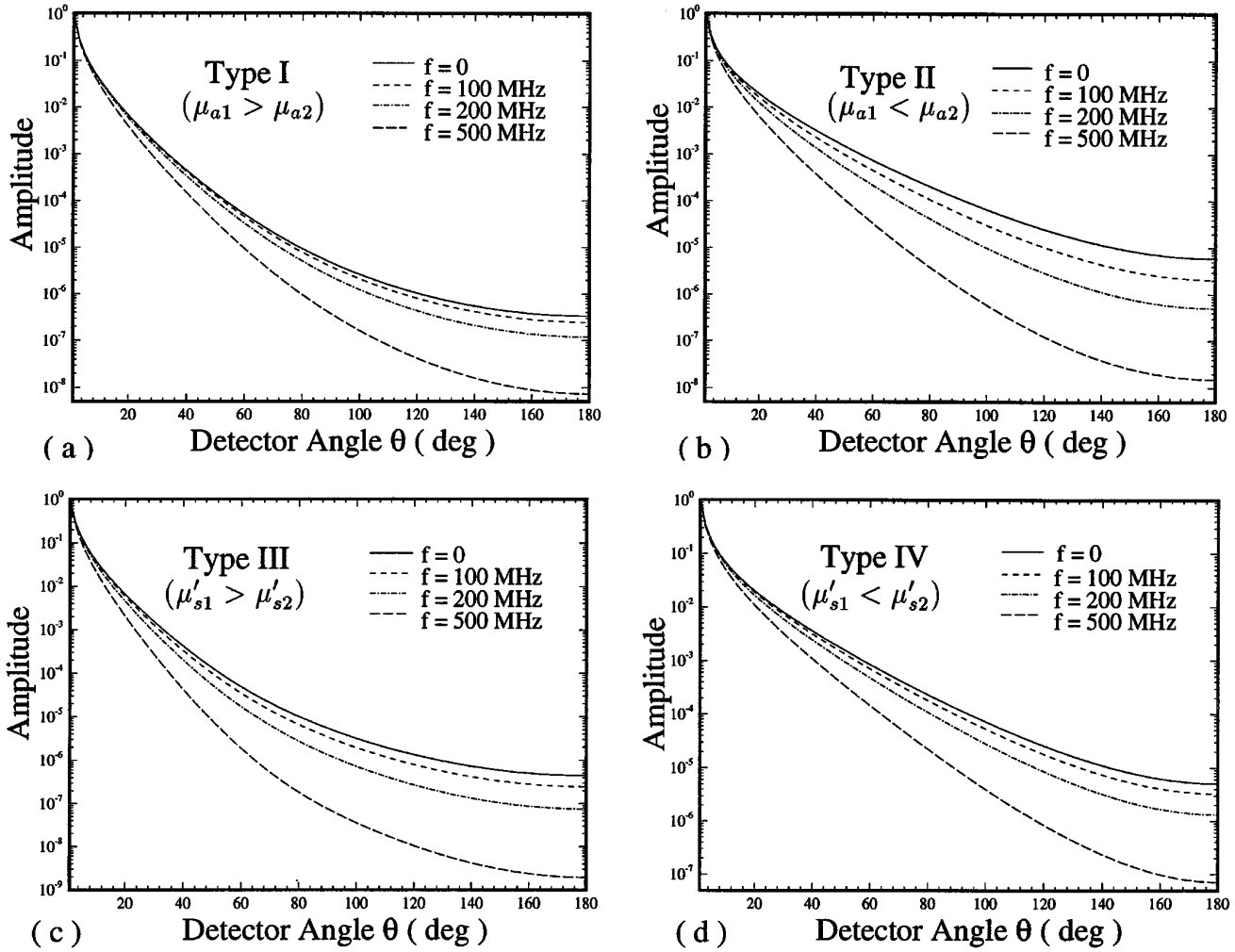

Fig. 2. Plots of the amplitudes of the background field for types I–IV of the background media versus the detector angle for several modulation frequencies ($f = 0$, for dc). The optical properties of the background media are listed in Table 1.

first kind, respectively[16]; P_n^m is the associated Legendre function; $\delta_m = 1$ for $m = 0$; and $\delta_m = 2$ for $m \geq 1$.

Substituting Eqs. (9)–(13) into Eqs. (6)–(8) and using appropriate boundary conditions, we find the coefficients A_{mn} in Eq. (10) are the ratios of two 4×4 determinants:

$$A_{mn} = \frac{\begin{vmatrix} A_1^* & a_{12} & a_{13} & 0 \\ A_2^* & a_{22} & a_{23} & 0 \\ 0 & a_{32} & a_{33} & a_{34} \\ 0 & a_{42} & a_{43} & a_{44} \end{vmatrix}}{\begin{vmatrix} a_{11} & a_{12} & a_{13} & 0 \\ a_{21} & a_{22} & a_{23} & 0 \\ 0 & a_{32} & a_{33} & a_{34} \\ 0 & a_{42} & a_{43} & a_{44} \end{vmatrix}}, \tag{14}$$

where the 14 nonvanishing elements a_{ij}, A_1^*, and A_2^* are listed in Appendix A.

In this paper, we use $|G_t|$ and Φ_t to represent the magnitude and the phase, respectively, of the total field when the object is present, and $|G_b|$ and Φ_b, respectively, when the object is absent (i.e., the background medium). The total field for the background medium is referred to as the background field. The difference between the total field in the presence of an object and the background field is the scattered field from the object. The background field here plays the same role as the incident field does when one studies the scattering that is due to an object embedded in a homogeneous background. In the following, we measure the sensitivity of a detector to a hidden object by the relative amplitude change δ_G and the phase change δ_Φ. These are defined as

$$\delta_G = 1 - \frac{|G_t|}{|G_b|}, \tag{15}$$

$$\delta_\Phi = \Phi_b - \Phi_t, \tag{16}$$

respectively.

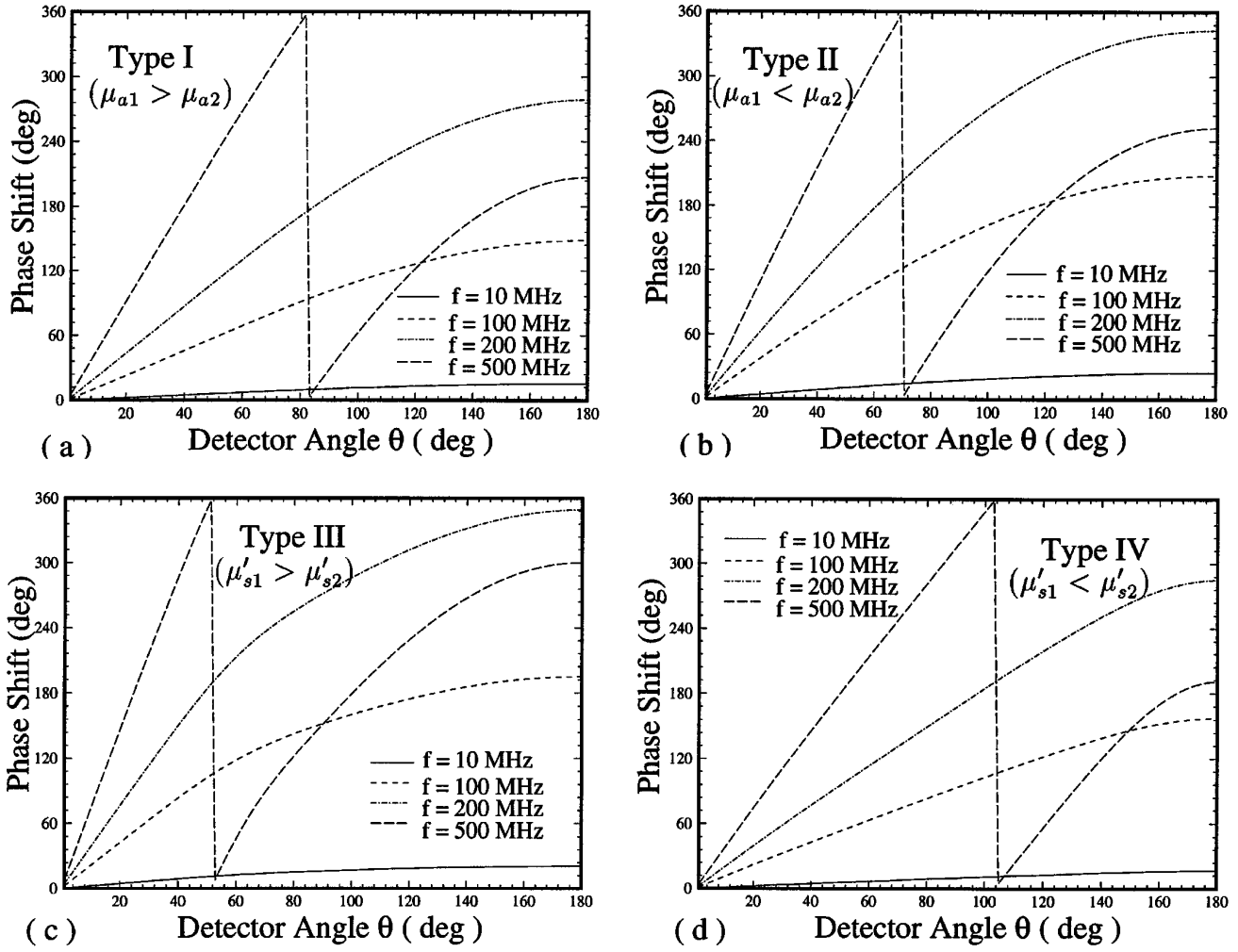

Fig. 3. Plots of the phase shift of the background field for types I–IV of the background media versus the detector angle for several modulation frequencies. The optical properties of the background media are listed in Table 1.

The absorption and scattering coefficients of the four different test media are listed in Table 1. The geometries of these background media are identical, with the radii of the inner and outer layers being $b = 3$ cm and $c = 4$ cm, respectively. Further, the absorption and scattering coefficients of the inner layer are fixed at $\mu_{a2} = 0.04\ \text{cm}^{-1}$ and $\mu'_{s2} = 10\ \text{cm}^{-1}$. Note that the background media differ only in the absorption and scattering coefficients of the outer layer. The diameters of these media, in units of transport mean-free path lengths, are approximately 80 for types I and II, and 100 and 70 for types III and IV, respectively. In some cases, variations in object properties increase these values by up to an additional 10 tmfp. As will be seen, these four types of background media lead to somewhat different conclusions with respect to the detector's sensitivity to embedded objects.

For each background medium, we try to answer four questions: (1) At which modulation frequency f is the amplitude $|G_b|$ of the background field large enough to be measured reliably, while the changes δ_G and δ_Φ, which are due to the presence of an object, are detectable as defined below? Based on the study of question 1, we select a modulation frequency for use in studying the other three problems. (2) For a fixed modulation frequency and fixed object properties, what is the radius, $a_{\min}$, of the smallest detectable object? (3) For a fixed modulation frequency and a fixed object size, what is the smallest detectable relative change in absorption, $\delta_{a,\min} = (\mu_{a3} - \mu_{a2})/\mu_{a2}$? (4) Similarly, what is the smallest detectable relative change in scattering, $\delta_{s,\min} = (\mu'_{s3} - \mu'_{s2})/\mu'_{s2}$? In answering these questions, we define a detectable signal as one for which the amplitude of the scattered field is no smaller than $|G_{\min}| = 10^{-10}$. In addition, the relative change in amplitude and the absolute change in phase must be greater than or equal to $\delta_{G,\min} = 0.1\%$ and $\delta_{\Phi,\min} = 0.1°$, respectively. These two requirements lead to a third condition, which is that the magnitude of the background field must be no smaller than $|G_{b,\min}| = 10^{-7}$. The derivation of these values is based on state-of-the-art optical instrumentation. Similar assumptions have been used by others working in this field.[5,17]

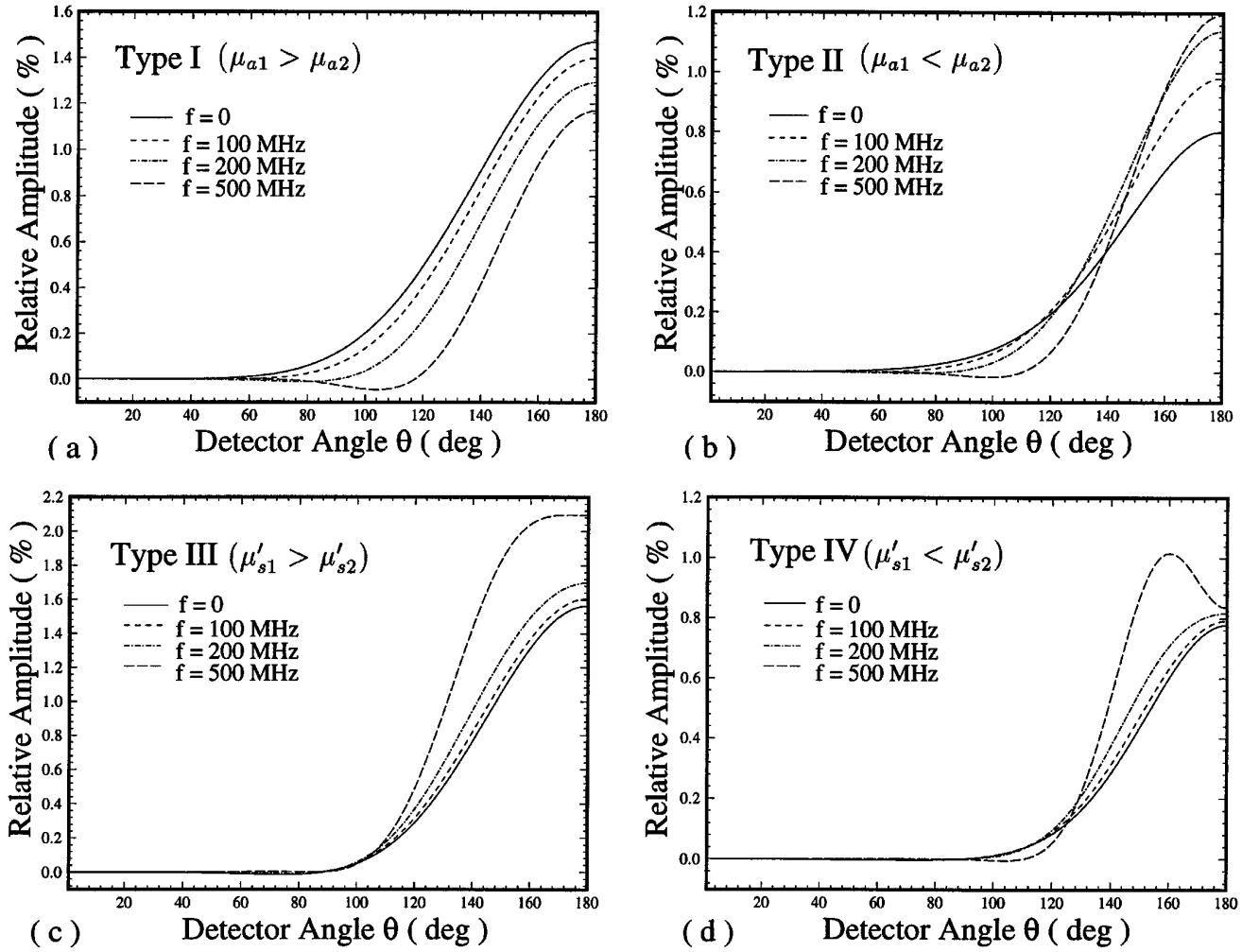

Fig. 4. Plots of the percent change in the amplitude versus the detector angle for different modulation frequencies, as attributed to an 0.5-cm-radius object, with $\mu_{a3} = 0.06\ \text{cm}^{-1}$ and $\mu'_{s3} = 10.0\ \text{cm}^{-1}$, embedded in types I and II background media and with $\mu_{a3} = 0.04\ \text{cm}^{-1}$ and $\mu'_{s3} = 15.0\ \text{cm}^{-1}$ embedded in types III and IV background media.

Although the solution presented above can be used to derive the total field at any point for an arbitrary source position, we present only the distribution of the total field on the surface of the outer layer at $r = c$ as a result of a source located on the same surface at $r' = c$, then $\phi = \theta = 0°$. Further, because of spherical symmetry, only detector responses on a half-circle defined by $r = c$, $\phi = 0°$, and $\theta = 0° - 180°$ are calculated. The detector at $\theta = 180°$ is opposite the source on the other side of the sphere. Using the solution above, we have computed the background fields for different background media and modulation frequencies, and, for a fixed background and a fixed modulation frequency, the total fields for different object sizes and object properties. In the next section, for each background medium, we first plot the amplitude $|G_b|$ and the phase shift Φ_b of the background field (Fig. 2). We then show the relative changes in amplitude δ_G and phase shift δ_Φ that are due to an embedded object (Fig. 3). Both sets of figures are drawn for different modulation frequencies and are used to derive the answer to the first question. Next, we show the δ_G and δ_ϕ plots for different object sizes and object properties (Figs. 4 and 5). These figures are meant to answer the other three questions. All plots are drawn as functions of the detector angle θ to evaluate the spatially dependent detector sensitivity to a hidden object. We have also calculated the minimum detectable object size and the relative changes in absorption and scattering for the detector angle that has the maximum sensitivity (i.e., the maximum change in amplitude or phase shift). The reader can derive the answers from the presented plots for other detector angles.

In our calculations, we assumed that the indices of refraction n_i of the different layers are $n_1 = n_2 = n_3 = 1.4$, following Bolin *et al.*[18] The speeds of light in these layers are, correspondingly, $v_1 = v_2 = v_3 = 2.14 \times 10^{10}$ cm/s.

3. Results

A. Influence of the Modulation Frequency

To determine the optimal modulation frequency for different background media, we have evaluated the

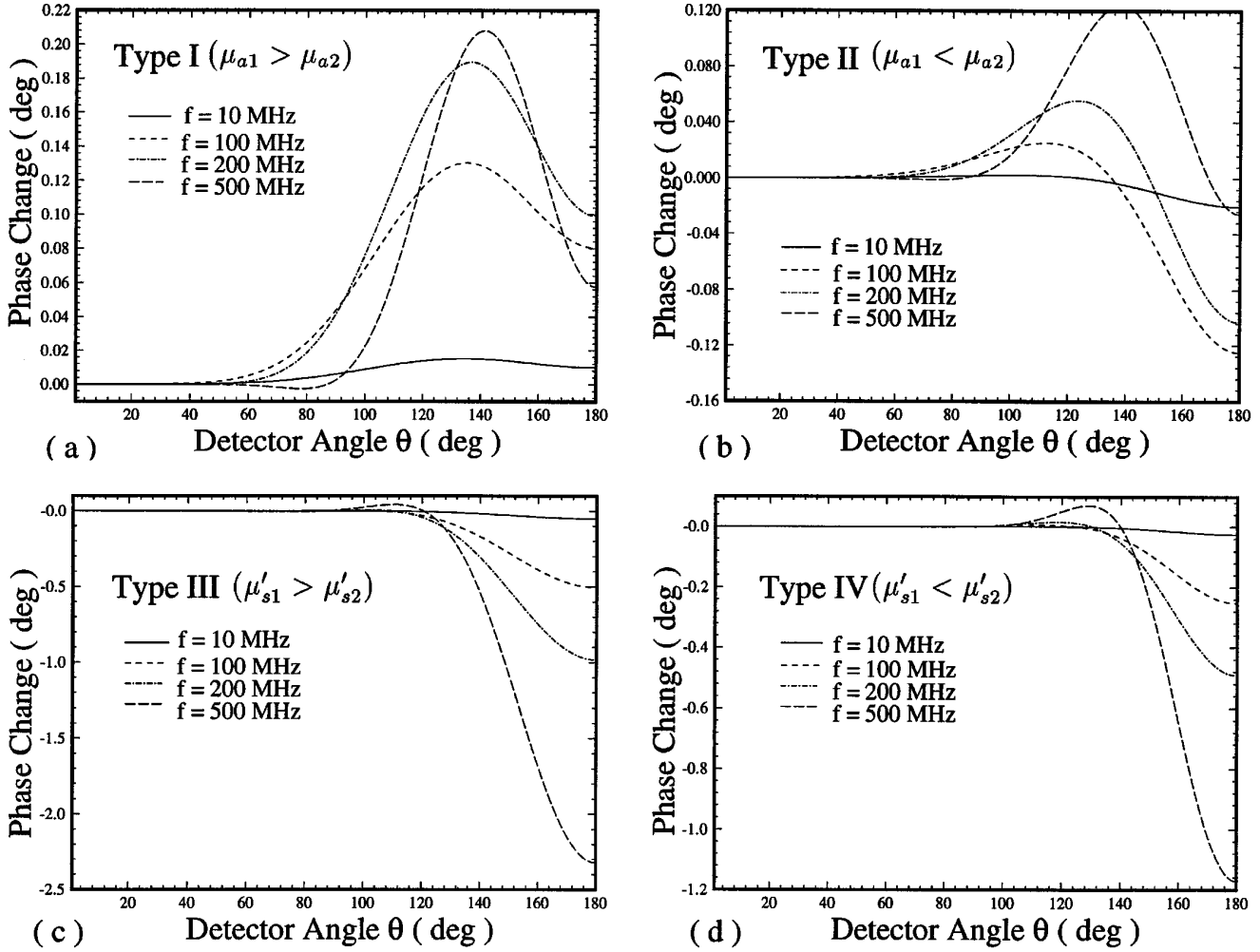

Fig. 5. Plots of the phase change in degrees versus the detector angle for different modulation frequencies, as attributed to a 0.5-cm-radius object, with $\mu_{a3} = 0.06$ cm^{-1} and $\mu'_{s3} = 10.0$ cm^{-1}, embedded in types I and II background media, and with $\mu_{a3} = 0.04$ cm^{-1} and $\mu'_{s3} = 15.0$ cm^{-1}, embedded in types III and IV background media.

amplitude and phase of the total field, with and without the object present, for several frequencies: $f = 0, 100, 200, 500$ MHz. The value $f = 0$ applied to dc. In Figs. 2 and 3 we show the amplitude and phase distributions of the background field as a function of the detector angle at these modulation frequencies for each of the four background media tested. As expected, the amplitude of the background field falls as the detector angle increases at a fixed frequency or as the frequency increases at a fixed detector angle. For example, for the type-I medium at detector angle $\theta = 180°$, the amplitude is 3.5×10^{-7} when $f = 0$. This value falls to $10^{-7} \approx |G_{b,\min}|$ when $f = 200$ MHz and to $8 \times 10^{-9} < |G_{b,\min}|$ when $f = 500$ MHz. The amplitude is greatest for a dc incident field. The background-field amplitudes for type-I and type-III media are approximately 10–100-fold smaller than those for types II and IV because of the stronger absorption or scattering in the outer layer. Figure 3 shows an increased phase shift with an increasing detector angle or a higher modulation frequency.

Figures 4 and 5 show the relative amplitude and phase change caused by a 0.5-cm-radius object with $\mu_{a3} = 0.06\ \text{cm}^{-1}$ and $\mu'_{s3} = 10.0\ \text{cm}^{-1}$ that is embedded in types-I and -II background media, and the same object but with $\mu_{a3} = 0.04\ \text{cm}^{-1}$ and $\mu'_{s3} = 15.0\ \text{cm}^{-1}$, embedded in types-III and -IV background media. It can be seen that the relative amplitude and phase changes are small when the detector angle is $<60°$. This is because the background field is much stronger than the scattered field at these angles. At larger detector angles, the changes are more visible and vary in a nonlinear manner with the detector angle. In most cases the change in amplitude increases approximately monotonically with the detector angle. For the type-I background medium, we observe that the amplitude sensitivity decreases with an increasing modulation frequency and the dc component has the greatest amplitude sensitivity. Interestingly, nearly the opposite trend is seen in all other background-media types. An unusual observation is the occurrence of a peak in the relative amplitude change for type-IV media at a 500-MHz modulation frequency and large detector angles. Overall qualitatively, we observed that, whereas there is some dependence of the amplitude responses on the type of background medium as a function of

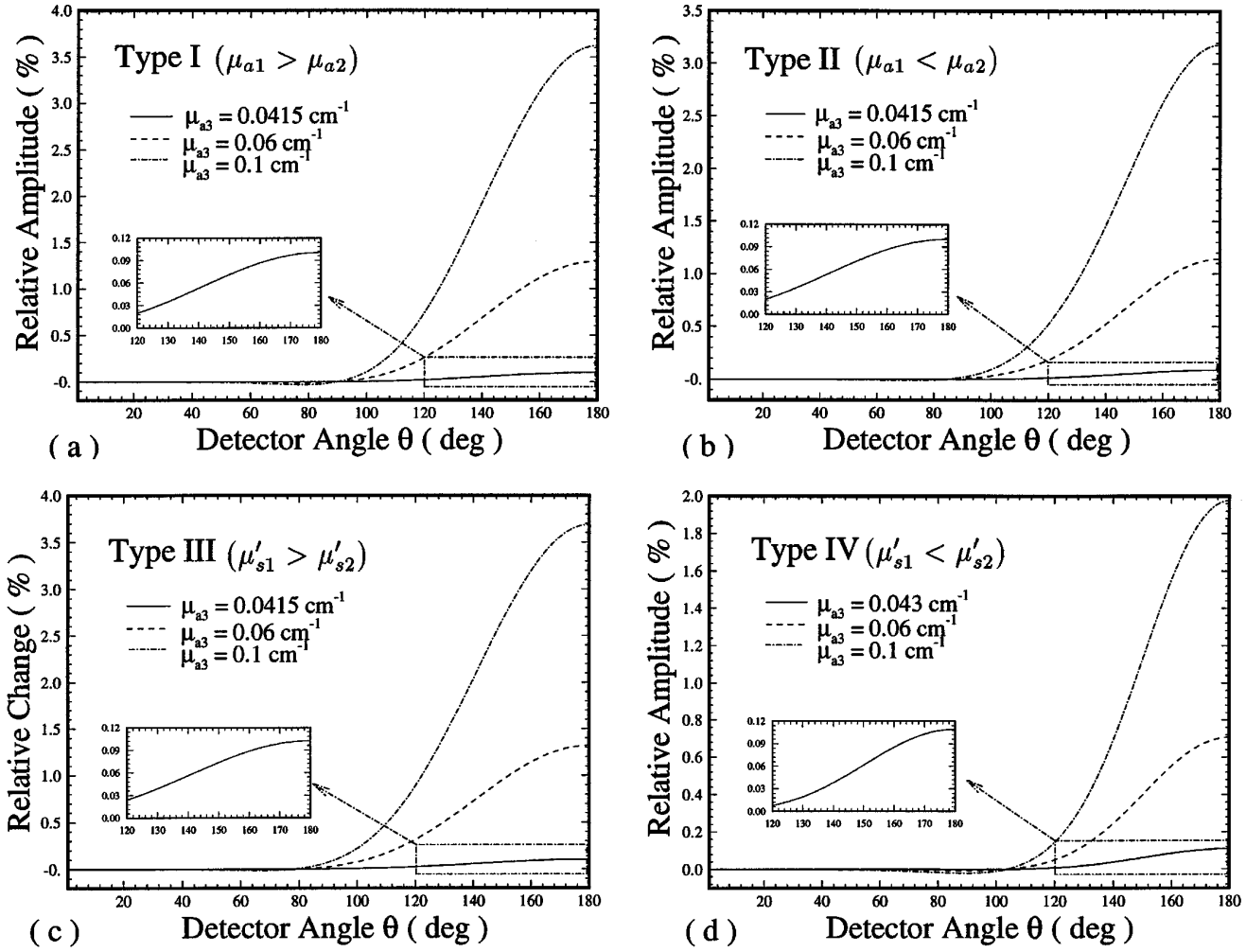

Fig. 6. Percent change in amplitude plotted versus the detector angle for different absorption coefficients μ_{a3} of an object with a radius of 0.5 cm and $\mu'_{s3} = 10.0\ \text{cm}^{-1}$, embedded in the types I–IV background media. The modulation frequency is 200 MHz.

the modulation frequency, no consistent pattern is evident.

The change in phase due to the presence of the object is shown in Figs. 5. These data show that when an absorption-coefficient gradient exists (types-I and -II background media), a peak in the phase plot is seen at intermediate detector angles (120°–140°). The amplitude and position of this peak vary with the frequency of modulation, with higher positive values observed for higher frequencies. For type-II media we also observed that the algebraic sign of the phase change becomes negative at a certain detector angle, which is a function of the modulation frequency. A qualitatively different trend is observed for background media having a scattering-coefficient gradient (types III and IV). Little to no intermediate peak is seen and, at larger detector angles and higher modulation frequencies, the phase changes are increasingly negative.

A quantitative comparison of the responses observed for different background media reveal an unexpected result: The amplitude and phase changes seen in type-I and type-III media are greater, respectively, than those seen for type-II and type-IV background media. The former two media have larger absorption- and scattering-coefficient values, respectively, in the outer layer, than do Types-II and -IV media. Note that the difference in amplitude sensitivity is also seen for a dc source. This finding for the type-III media is particularly noteworthy if it is considered that the diameter of this medium is almost 50% greater than that of the type-IV medium. Thus, we are observing greater sensitivity to the object even though the absolute amplitude of emerging light is significantly less than for the type-IV medium, e.g., approximately 14 times less at $\theta = 180°$ [see Figs. 2(c) and 2(d)]. Possible explanations, described in more detail in Section 4, include a selective suppression of detected photons that remain in the outer layer, the trapping of photons in the inner layer, or a combination of these.

Based on the criterion that the amplitude of the background field should be greater than $|G_{b,\min}| = 10^{-7}$, the modulation frequencies that achieve the optimal compromise between signal strength and

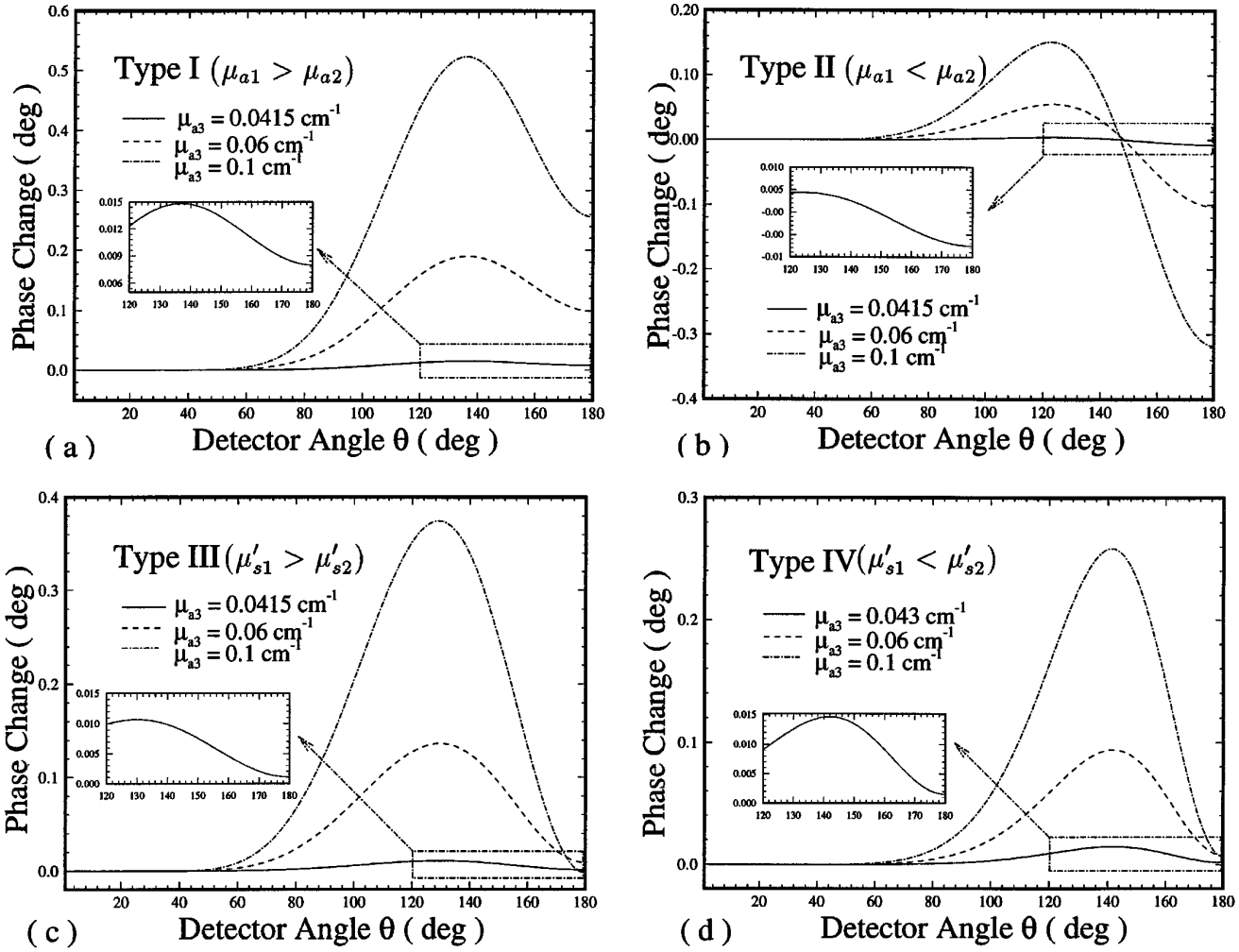

Fig. 7. Phase change in degrees plotted versus the detector angle for different absorption coefficients μ_{a3} of an object with a radius of 0.5 cm and $\mu'_{s3} = 10.0$ cm^{-1}, embedded in types I–IV background media. The modulation frequency is 200 MHz.

Table 2. Optimal Modulation Frequency, Minimum Detectable Object Radius, and Absorption and Scattering Variations for Background Media Types I–IV

Medium Type	f_{opt} (MHz)	Detectable Signal Change: Signal Type	Detectable Signal Change: Amount of Change	Object Radius[a]: θ	Object Radius[a]: a_{min} (cm)	Absorption and Scattering Variation[b]: θ	Absorption and Scattering Variation[b]: $\delta_{a,min}$ (%)	Absorption and Scattering Variation[b]: θ	Absorption and Scattering Variation[b]: $\delta_{s,min}$ (%)
I	200	δ_G	≥0.1%	180°	0.22	180°	3.75	180°	2.0
	200	δ_Φ	≥0.1°	140°	0.40	140°	25.0	180°	5.0
II	300	δ_G	≥0.1%	180°	0.25	180°	5.0	180°	4.0
	300	δ_Φ	≥0.1°	180°	0.50	180°	50.0	180°	4.0
III	200	δ_G	≥0.1%	180°	0.20	130°	12.5	180°	2.5
	200	δ_Φ	≥0.1°	180°	0.23	130°	37.5	180°	4.0
IV	500	δ_G	≥0.1%	180°	0.25	140°	20.0	180°	4.5
	500	δ_Φ	≥0.1°	180°	0.30	140°	50.0	180°	8.0

[a] $\delta_a = 50\%$; $f = 200$ MHz.
[b] $a = 0.5$ cm; $f = 200$ MHz.

relative response are approximately 200, 300, 200, and 500 MHz for types-I–IV background media, respectively. For comparison purposes, however, we chose a frequency of 200 MHz for all the background media in the following studies.

B. Effect of Variations in the Absorption Coefficient of the Object

The results shown in Figs. 6 and 7 show the computed sensitivities to a change in the object's absorption coefficient as a function of the detector angle for

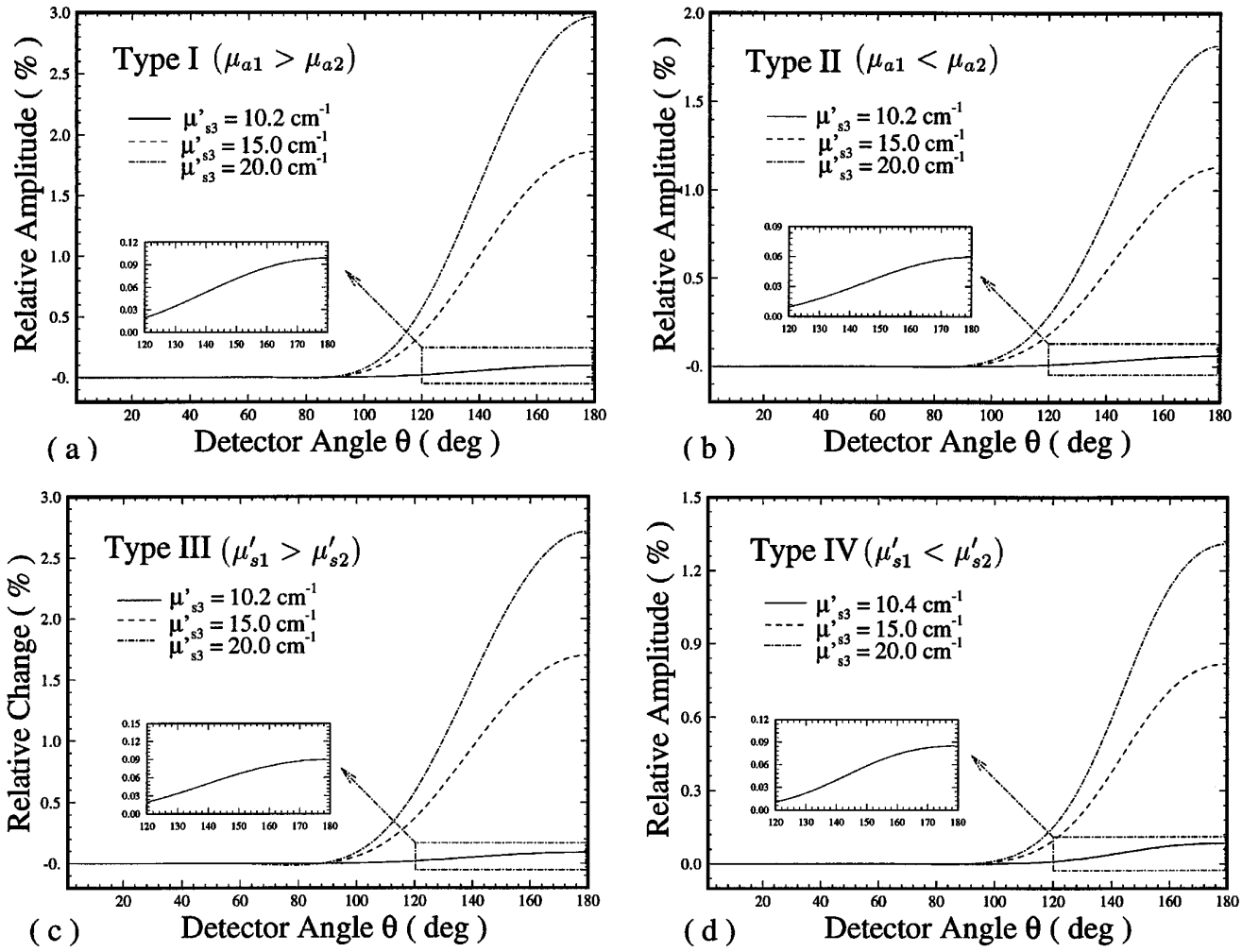

Fig. 8. Percent change in amplitude plotted versus the detector angle for different scattering coefficients μ'_{s3} of an object with a radius of 0.5 cm and $\mu_{a3} = 0.04$ cm^{-1}, embedded in types I–IV background media. The modulation frequency is 200 MHz.

each of the background media tested. For these studies the size of the object and its scattering coefficient are fixed at $a = 0.5$ cm and $\mu_s' = 10$ cm^{-1}, respectively. In each case, the absorption coefficient of the object was varied over a range of approximately 0.04–0.1 cm^{-1}. At increasing detector angles and μ_a values, the change in amplitude increases monotonically in a nonlinear fashion. Figures 7 show that an absorption perturbation produces a peak in the phase plot at intermediate detector angles (120°–140°). The amplitude and position of this peak vary with the object's μ_a, with the maximum absolute phase shift increasing as μ_a increases. For type-II media we also observe that at detector angles >140°, the algebraic sign of the phase change becomes negative and is a function of μ_a. Further inspection shows, interestingly, the existence of an isosbestic point at $\theta \approx 145°$, indicating that at this angle the detector is insensitive to a change in the absorption coefficient of the object. (In spectroscopy the term isosbestic point refers to a wavelength at which variations in the ratio of two compounds in equilibrium do not produce any change in the net absorbance. We borrowed the term here because we observed that at a specific angle the measured phase is independent of the value of the object's absorption coefficient in one instance or of its radius in another.) A quantitative comparison of the phase shift and the relative changes in amplitude for the different media reveals a greater sensitivity to absorption perturbations in the object for types-I and -III media. By interpolating the data in these plots, we determine that the smallest detectable absorption perturbation varies from approximately 0.0015 to 0.005 cm^{-1} (3.75–12.5%) for amplitude measurements and from 0.01 to 0.02 cm^{-1} (25–50%) for phase measurements, depending on the properties of the background medium. See Table 2.

C. Effect of Variations in the Scattering Coefficient of the Object

The results in Figs. 8 and 9 show the computed sensitivities to a change in the object's scattering coefficient as a function of the detector angle for each background medium tested. Note that for these studies the size of the object and its absorption coefficient are fixed at $a = 0.5$ cm and 0.04 cm^{-1}, respectively. In each case the scattering coefficient

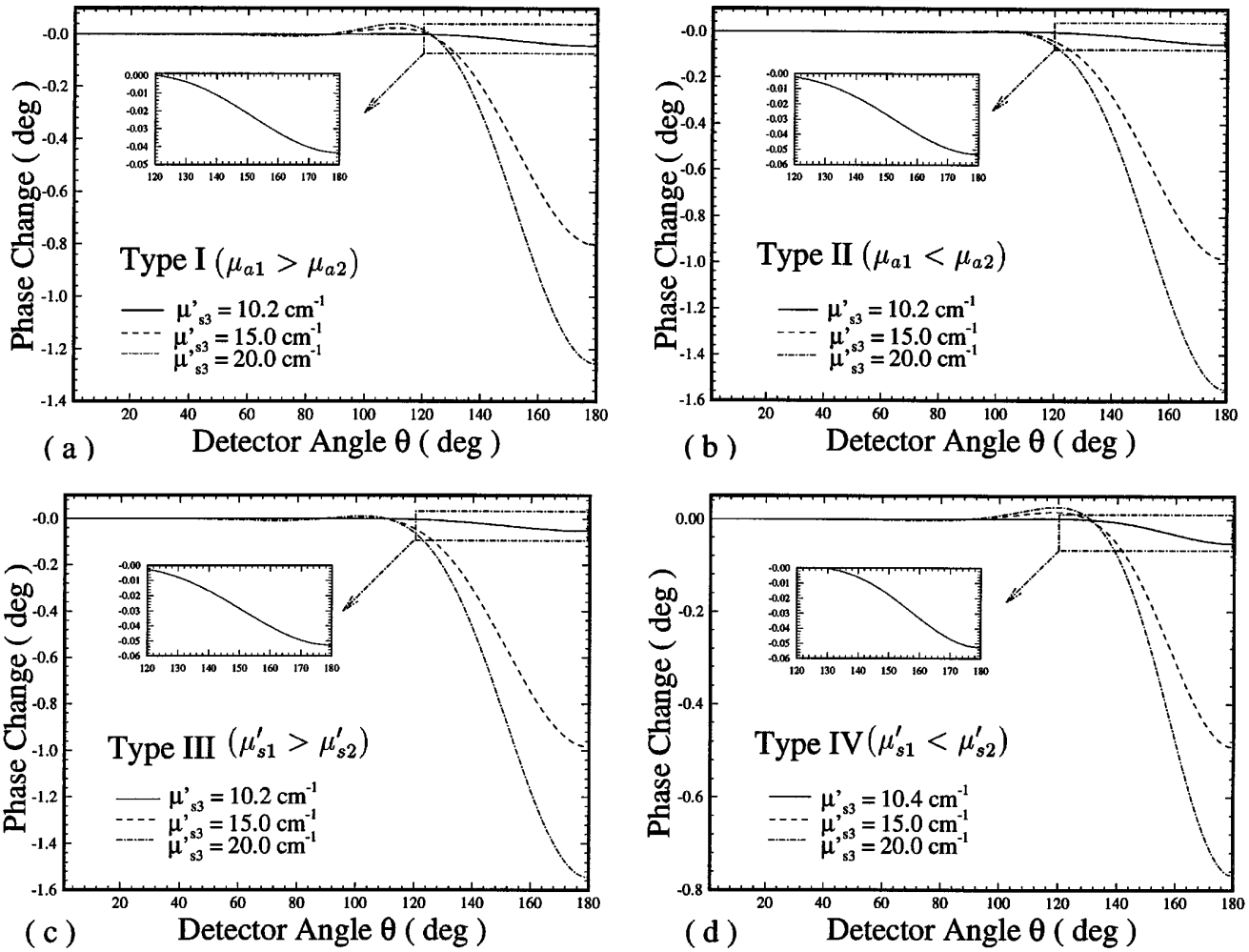

Fig. 9. Phase change in degrees plotted versus the detector angle for different scattering coefficients μ_{s3}' of an object with a radius of 0.5 cm and $\mu_{a3} = 0.04$ cm^{-1}, embedded in types I–IV background media. The modulation frequency is 200 MHz.

of the object was varied over a range of approximately 10–20 cm^{-1}. A qualitative examination of the amplitude and phase plots reveals little difference in the responses seen for different media. In all cases, an increase in the scattering coefficient of the object produces a nonlinear, monotonic increase in the relative amplitude change, with larger differences seen at larger detector angles. A qualitatively similar response is seen in the phase data. In this case, the phase change becomes increasingly more negative at larger detector angles and for larger values of the object's scattering coefficient. By linearly interpolating the data for other intermediate values of μ'_{s3}, we have found that the smallest detectable change, $\delta_{s,\min}$, at $\theta = 180°$, varies from 0.2 to 0.45 cm^{-1} (2–4.5%) for amplitude measurements and from 0.4 to 0.8 cm^{-1} (4–8%) for phase measurements. See Table 2.

A comparison of the responses in the phase and amplitude data produced by a perturbation in absorption (Figs. 6 and 7) to a perturbation in scattering (Figs. 8 and 9) shows important qualitative and quantitative differences. Qualitatively, we observe that, unlike the trends seen in the amplitude data, the phase data show distinctly different responses to absorption- and scattering-coefficient perturbations. A quantitative comparison reveals that amplitude measurements are proportionally more sensitive to a change in absorption, whereas phase measurements are proportionally more sensitive to a change in scattering. In absolute terms, however, we observed that in all cases amplitude measurements are more sensitive than phase measurements. Further inspection reveals that the trends seen in the phase data can be further influenced by differences in the optical properties of the outer layer. A comparison of the phase data obtained from type-I and type-III media shows that an absorption perturbation causes a greater phase change for a type-I medium, whereas a scattering perturbation causes a larger phase shift for a type-III medium.

D. Effect of Variations in the Object Diameter

The results shown in Figs. 10 and 11 show the computed sensitivities to a change in the object's size as a function of the detector angle for each of the

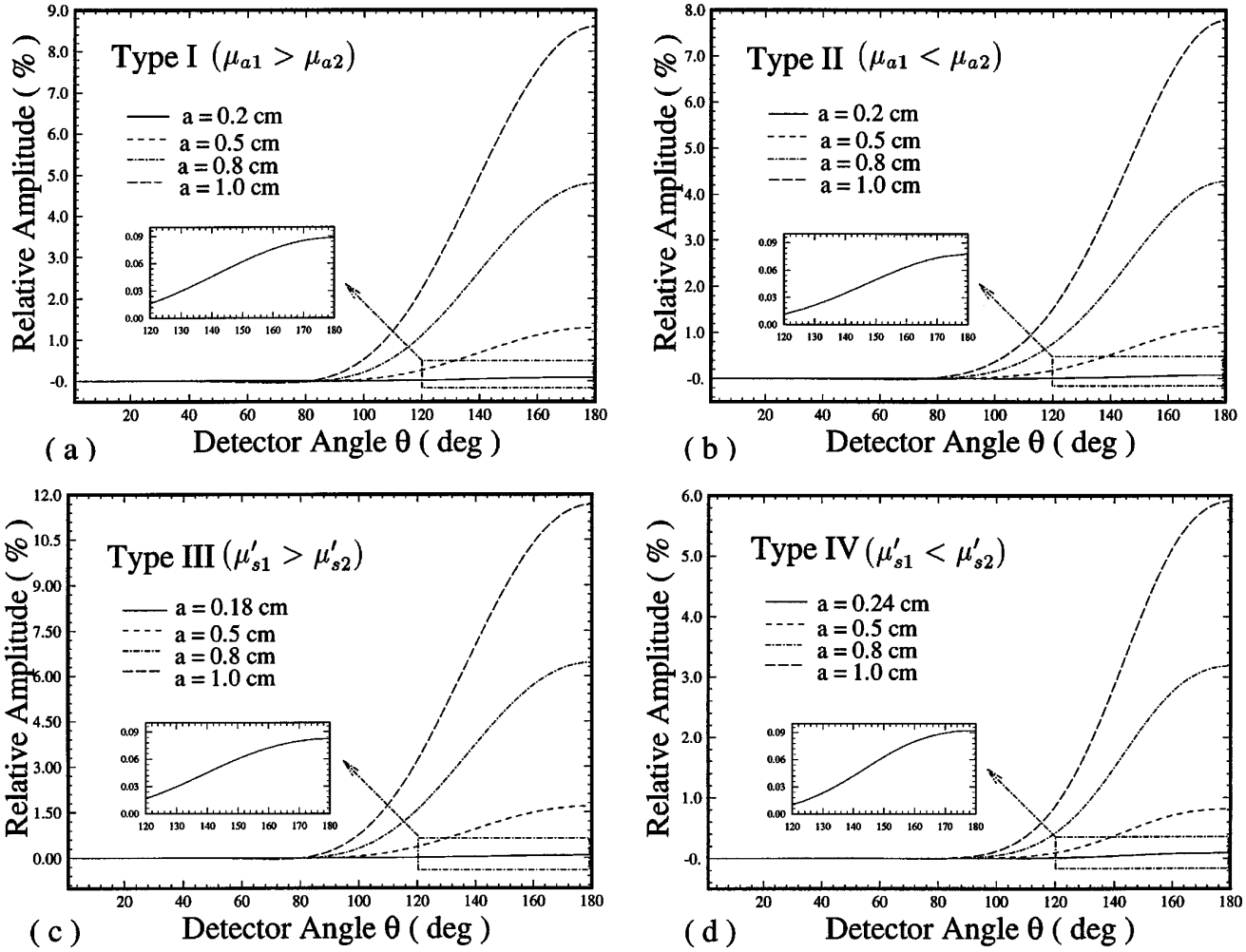

Fig. 10. Percent change in amplitude plotted versus the detector angle for different radii a of an object with $\mu_{a3} = 0.06$ cm^{-1} and $\mu'_{s3} = 10.0$ cm^{-1}, embedded in types I and II background media and with $\mu_{a3} = 0.04$ cm^{-1} and $\mu'_{s3} = 15.0$ cm^{-1}, embedded in types III and IV background media. The modulation frequency is 200 MHz.

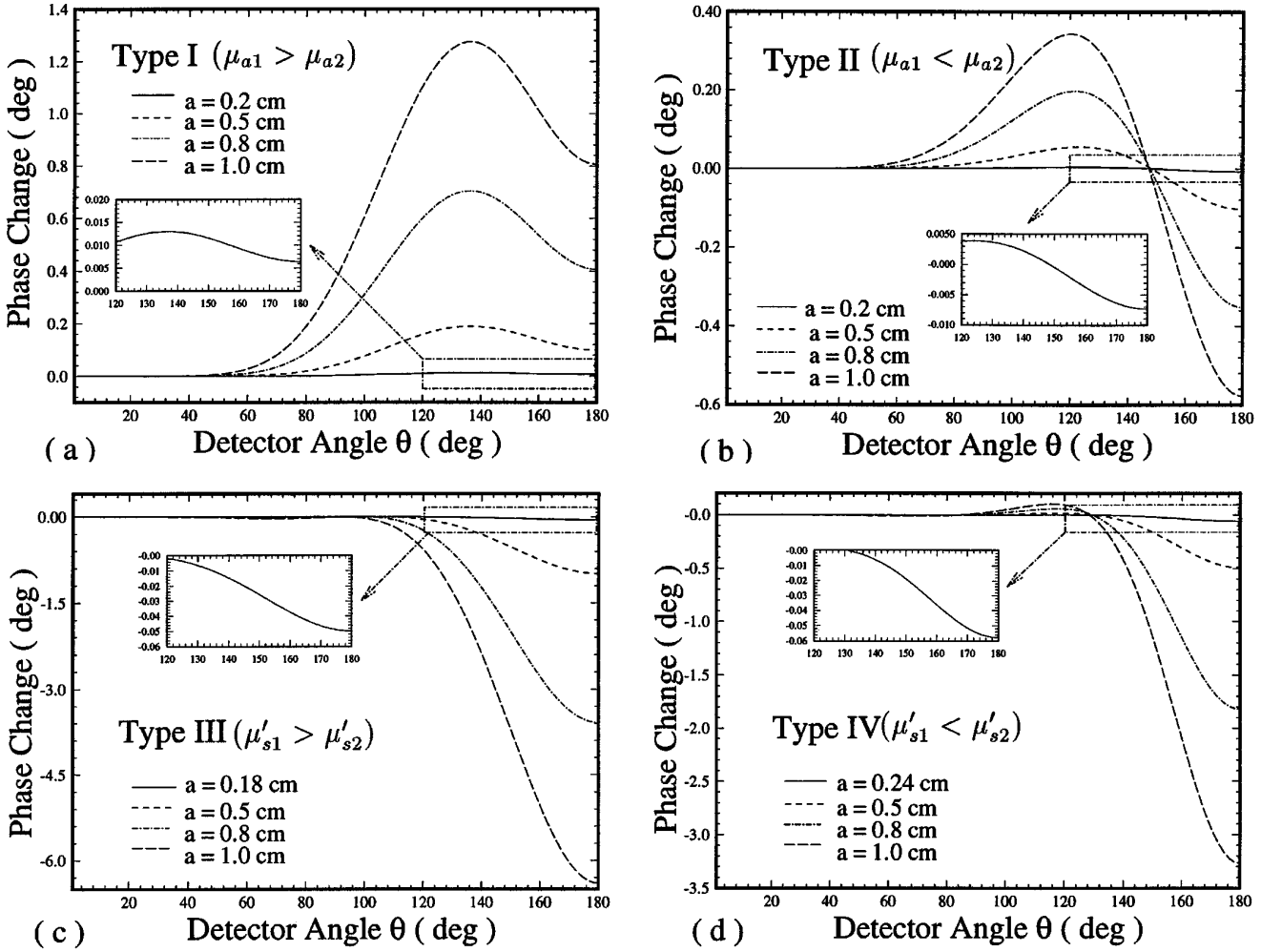

Fig. 11. Phase change in degrees plotted versus the detector angle for different radii a of an object with $\mu_{a3} = 0.06\ \text{cm}^{-1}$ and $\mu'_{s3} = 10.0\ \text{cm}^{-1}$, embedded in types I and II background media, and $\mu_{a3} = 0.04\ \text{cm}^{-1}$ and $\mu'_{s3} = 15.0\ \text{cm}^{-1}$, embedded in types III and IV background media. The modulation frequency is 200 MHz.

background media tested. For these studies, the absorption and scattering coefficients of the object are fixed: for types-I and -II media, $\mu_{a3} = 0.06\ \text{cm}^{-1}$ and $\mu'_{s3} = 10.0\ \text{cm}^{-1}$, respectively; for types-III and -IV media, $\mu_{a3} = 0.04\ \text{cm}^{-1}$ and $\mu'_{s3} = 15.0\ \text{cm}^{-1}$. Thus, for a specified object size, only μ_{a3} is perturbed in Types-I and -II media, and only μ'_{s3} is perturbed in types-III and -IV media. The radius of the object was varied from approximately 0.2 to 1.0 cm. As was the case for the other perturbations, inspection of the amplitude data reveals few or no qualitative differences in the responses seen for the different medium types. At increasing detector angles and object sizes, the change in amplitude increases monotonically in a nonlinear fashion. A similar comparison for the phase data, however, shows a qualitatively different response. For types-I and -II media, a perturbation in object size produces a peak in the phase plot at intermediate detector angles, 120°–140°. The amplitude and position of this peak vary with the object size, with higher positive values observed for larger radii. In fact, the responses seen for both the amplitude and the phase data for types-I and -II media to a perturbation in object size appear qualitatively almost indistinguishable from those produced by a perturbation in the absorption coefficient (see Figs. 5 and 6). A qualitatively similar response is observed for types-III and -IV media with respect to the changes seen in the amplitude and phase plots for a perturbation in scattering (see Figs. 7 and 8). Interestingly, we also observe an isosbestic point in the phase data at $\theta \approx 145°$ for the type-II medium. These findings demonstrate that, when there is a gradient in only one parameter, this type of measurement does not readily distinguish between a change in the object's intensive properties (i.e., the coefficients) and a change in its extensive properties (i.e., the volume). Interpolation of the plotted data shows that the smallest detectable perturbation in the object radius varies from approximately 0.2 to 0.25 cm for amplitude data and from 0.23 to 0.5 cm for phase data, depending on the properties of the background medium. See Table 2.

4. Discussion and Conclusion

In this paper we have presented a detailed sensitivity study for the PDW for imaging a spherically symmetric, two-layer, highly scattering, infinite medium containing a spherical object. The changes in the amplitude and the phase of the total field that are caused by the object have been calculated as functions of the modulation frequency, the object radius, and the differences between the absorption and scattering coefficients of the object and the background. For each of the four different types of background media, we have derived the optimal modulation frequency, the smallest detectable object size, and the minimal detectable differences in absorption and scattering coefficients. The results are summarized in Table 2. The quantitative results are based on certain assumptions concerning the precision of commercially available optical detectors. For a different set of detector precisions, one can easily derive corresponding results from the plots presented in Figs. 4–11.

A. Comparison of Background-Media Types I–IV

A comparison of the corresponding figures for the different background media permits the following interesting points to be observed:

1. Increasing μ_a or μ_s' in the outer layer results in an enhanced sensitivity to the embedded object. The suggestion that enhanced sensitivity to an embedded object can result from the presence of a more strongly absorbing or scattering outer layer has potentially important implications for experimental studies. Should this effect prove to be significant in practice, one could easily consider placing a balloon filled with a strongly absorbing or scattering medium around the test medium being investigated. The balloon could be constructed to permit optical fibers to be in direct contact with a target tissue and, in doing so, act to trap photons that would ordinarily have exited the medium at the air–tissue interface by reflecting them back into the medium.
2. More information is gained about the inhomogeneity if frequency-domain light-detection techniques are used to acquire data for image reconstruction. To obtain a good spatial resolution, one must increase the modulation frequency. The optimal modulation frequency depends on the background-medium properties. For all media except type I, the sensitivity of the detected light to the embedded object increases with an increasing modulation frequency.
3. Whereas the absolute sensitivity of the amplitude measurements is greater than that of the phase measurements to changes in the absorption and scattering properties of an embedded object, the former measurements are relatively insensitive to the type of perturbation. Phase measurements, on the other hand, exhibit a much greater ability to distinguish absorption perturbations from scattering perturbations.
4. Amplitude measurements are proportionally more sensitive to absorption changes, whereas phase measurements are proportionally more sensitive to scattering changes.
5. Evidence of degenerate detector responses was observed under several of the conditions tested. This phenomenon may contribute to the difficulty of quantification of the absolute optical coefficients of tissue by the use of simplified measurement and analysis schemes.

A possible physical interpretation of some these findings is depicted in Fig. 12. Illustrated are two classes of photon paths: those that interact with the object at some point along their path (class I), and those that do not interact but can still enter the detector (class II). Point 1 above is explained if we recognize that increasing μ_a in the outer layer preferentially removes class-II photons because this group includes those having the longest paths in the outer layer. This removal serves to increase the fraction of detected photons that interact with the object, thus enhancing the sensitivity to the object. A somewhat similar explanation holds for the observed effect of increased scattering in the outer layer on the object's detectability. Here, preferential removal of class-II photons occurs because, as scattering increases, the probability that scattered photons will ultimately enter the detector is reduced. In essence, once photons are removed, it becomes more difficult for the scattered photons to come back. An alternative explanation is that the presence of a

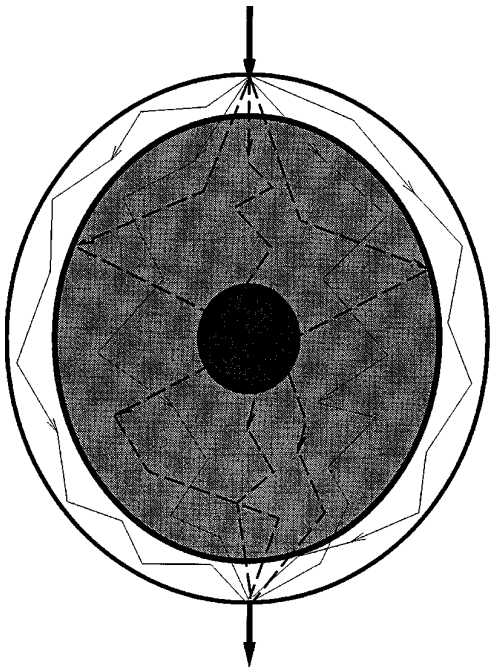

Fig. 12. Illustration of two classes of photon paths. Class-I photons (dashed photon paths) interact with the object (darkest circle, at the center) at some point along their path. Class-II photons (solid photon paths) do not interact with the object but can still enter the detector.

more-scattering outer layer could serve to trap those photons that enter the inner layer, permitting greater interaction with the object.

The findings listed under point 2 above regarding the frequency dependence of the object's detectability on the background-medium type follow from the variation that can be reasonably expected in detector response with the changing overall (i.e., averaged over the medium) attenuation. Thus, because types-I and -III media attenuate the propagating signal more in the outer layer than do types II and IV, it can be expected that, for a specified sensitivity limit, higher modulation frequencies will remain measurable for the latter media types. This finding is independent of the photon class and is instead a function of detector sensitivity. We note, however, that this explanation cannot completely describe the observations. In particular, we point out that unlike types-II–IV media, the type I medium exhibits the greatest amplitude sensitivity to the object at zero frequency (dc).

In point 3 above, two observations are made: For a specified perturbation, amplitude measurements exhibit a greater absolute sensitivity, whereas phase measurements can distinguish between absorption and scattering perturbations. Phenomenologically, this means that a specified perturbation (absorption, scatter, or object size) influences the number of photons reaching a detector more than it does their time of arrival. The observation regarding the differential response of phase data is not unexpected. It occurs because the changes in scattering influence the mean time of photon arrival at a detector quite differently than do the changes in absorption.

Point 4 is explained as follows: Changes in the scattering coefficient influence the paths of essentially all photons migrating through a specified region. Corresponding changes in absorption, on the other hand, preferentially influence those photons having the longest paths. Therefore, it can be expected that phase measurements, which are proportional to the mean path length, will be more sensitive to variations in the scattering coefficient. The observation that amplitude measurements are preferentially sensitive to variations in the absorption coefficient can be explained if we consider that, whereas absorption removes photons, scattering causes their redistribution, allowing some to ultimately enter the detector.

In Figs. 7(b) and 11(b), an isosbestic point in the phase data is clearly evident. In light of the geometry of the media studied, we believe that this observation may be a special case. Basically, because the object is centrally located, increases in object size, for example, will decrease the time of arrival of the PDW at the object–inner-layer boundary in the hemisphere closest to the source and increase the arrival time in the hemisphere opposite the source. For a centrally located object, these differences might be expected to cancel at a particular point. If this argument is correct, an isosbestic point would be less likely to occur if the object was off center. For media containing multiple embedded objects such as tissue, however, isosbestic points might well occur as a result of the expected multiple interactions.

It is worthwhile to examine the results summarized in Table 2. Contrary to our initial expectations, the optimal sensitivity to the studied perturbations is not always associated with detectors located opposite the source ($\theta = 180°$). Instead, in many instances we observed the optimal sensitivity at intermediate angles in the forward hemisphere ($90° < \theta \leq 180°$). We interpret this finding to indicate that, because of multiple scattering that results from the presence of two internal boundaries, partial cancellation of the scattered PDW's can occur in a position-dependent manner. The magnitude of this effect varies with the composition of the background medium, as the characteristics of scattered waves produced at the outer-layer–inner-layer boundary vary.

As noted above, we observed different sensitivities for the amplitude and phase data. In essentially all cases studied, amplitude measurements were more sensitive than phase measurements to perturbations in object size or absorption or scattering coefficients. As mentioned above, this difference indicates that such changes influence the number of arriving photons more than it does their mean arrival time. Interestingly, this difference in sensitivity seemed more pronounced for perturbations in absorption than in scattering or object size. For the cases studied, we find that, with a 50% contrast in absorption between the object and the inner layer, the smallest detectable object size is approximately 4 mm in diameter. As all media studied have optical coefficients in the range expected for most tissues, we believe that centrally located objects having this contrast and size should be detectable for tissue having a thickness of approximately 7.5–10.5 cm. Detection of even smaller off-center objects should be possible. Also shown in Table 2 are the contrast limits for a 1-cm-diameter, centrally located object. Generally, we observe a greater sensitivity to fractional changes in the scattering coefficient. Overall, the minimum perturbations required to produce a measureable change in a detector response are quite small. We also list the optimal frequency for the greatest sensitivity to the introduced perturbations, which varies between 200 and 500 MHz.

B. Implications of Results for Imaging Thick Tissues

A number of laboratories, including ours, are investigating the possibility of computing tomographic images of thick tissues on the basis of the detection of highly scattered optical photons.[8,19–22] Whereas we recognize that the conditions examined here are highly idealized, we believe our results should provide an estimate of the image quality that might be achieved. Real media such as breast tissue are highly inhomogeneous and have nonuniform bound-

aries. Air–tissue interfaces can be treated as perfect absorbers. Variations in tissue geometry, e.g., a compressed versus an uncompressed state, can lead to additional light losses. Taken together, it can be expected that, for tissues having an optical thickness equivalent to the media examined here, greater losses will be experienced. As a result, the accurate detection of these signals will require correspondingly higher source intensities. The sensitivity values reported in Table 2 correspond to an input-source intensity of 10^{14} photons/s, or 26.5 μW at 750 nm. Source intensities of 26.5 mW [10^{17} photons/s for a beam cross-sectional area of, say, 2 mm ($\approx$1 W/cm^2)] are easily tolerated at NIR frequencies by most nonocular tissues. Thus, we believe there is considerable room to accommodate the expected losses. This possible intensity range suggests that the sensitivity values listed in Table 2 may underestimate the achievable values to the extent that sensitivity is photon limited. Given that these values represent only a fraction of the absorption and scattering coefficients of most tissues, it is tempting to suggest that the results obtained here support the prospect of detecting relatively small changes in the optical coefficients for deeply buried anomalies by the use of frequency–domain methods. We recognize, however, that other sources of noise exist, in particular those arising from motion artifacts.

Recently Moon and Reintjes[23] have reported that, for media thicker than $\approx$35 tmfp, image resolution with diffuse light degrades approximately linearly, with a scale dependence of $R = 0.2d$, where R is the resolution and d is the distance between the object and detector. Note that this relation is a function of only distance and thus holds even for a perfect absorber. Comparison of this value with those of the media examined here ($\approx$70–100 tmfp) indicates that the smallest object located in the center that could be resolved is 0.7–1.0 cm in size. Coincidentally this value is on the higher end of the detection limits computed here. Taken together, and with the possible differences arising from the different source conditions used here neglected, these findings indicate that, for a single source and single projection, objects of this size and the contrast values listed in Table 2, which are quite small, might be resolved. We wish to emphasize, however, that the conclusion of Moon *et al.*,[23] while valid, does not pertain to resolution limits achievable by the use of tomographic-imaging schemes. Indeed, Graber *et al.*[24] have recently reported experimental results demonstrating edge-detection limits of $<$1 mm for reconstructed images of a single inclusion (a black rod) located in the center of a cylindrical vessel having an optical thickness of approximately 150–200 tmfp. This result was obtained from tomographic measurements with a time-independent laser source operating at 720 nm. Assuming a transport mean free path length value of 1 mm, these data yield a resolution 15–20 times greater than the theoretical limit achievable from a single projection.

The reason why tomographic methods are capable of yielding improved resolution is that the multiprojection algorithms of the type used by Graber *et al.*[24] basically represent a spatial-filtering technique. The best one can learn from a single projection is that an object lies somewhere along a particular path. Essentially, one knows where the object is (i.e., along the path) but not where it is *not* (i.e., which portions along the path it is not located). In a multiple-scattering medium, this path becomes blurred, causing a loss of resolution. With multiple projections, however, one is essentially able to determine where the object is not located. More formally, this filtering effect proceeds directly from the structure of the Jacobian matrix.[19]

We view the results presented here as being moderately encouraging regarding the prospect for developing practical imaging schemes for studying thick tissue structures. We wish to emphasize that many important issues remain to be addressed. Of particular concern is how best to deal with the difficult issue of ill posedness in the inverse problem. One approach we have recently begun to explore is the use of priors derived from magnetic-resonance data.[25] We choose the magnetic-resonance technique because of the excellent contrast it affords for soft tissues. By assigning optical coefficients to appropriately segmented images, one can derive potentially accurate reference states.

Appendix A.

The 14 nonvanishing elements appearing in Eq. (14) are as follows:

- $A_1^* = j_n(k_1 b)$,
- $A_2^* = k_1 D_1 j_n'(k_1 b)$,
- $a_{11} = -h_n^{(1)}(k_1 b)$,
- $a_{12} = j_n(k_2 b)$,
- $a_{13} = y_n(k_2 b)$,
- $a_{21} = -k_1 D_1 h_n^{(1)\prime}(k_1 b)$,
- $a_{22} = k_2 D_2 j_n'(k_2 b)$,
- $a_{23} = k_2 D_2 y_n'(k_2 b)$,
- $a_{32} = j_n(k_2 a)$,
- $a_{33} = y_n(k_2 a)$,
- $a_{34} = -j_n(k_3 a)$,
- $a_{42} = k_2 D_2 y_n'(k_2 a)$,
- $a_{43} = k_2 D_2 y_n'(k_2 a)$,
- $a_{44} = -k_3 D_3 j_n'(k_3 a)$.

This work was supported in part by the National Institutes of Health under grant RO1-CA59955, by Office of Naval Research grant N000149510063, and by the New York State Science and Technology Foundation.

References

1. J. Fishkin, E. Gratton, M. J. vandeVen, and W. W. Mantulin, "Diffusion of intensity modulated near-infrared light in turbid media," in *Time-Resolved Spectroscopy and Imaging of Tissues,* B. Chance and A. Kazir, eds., Proc. Soc. Photo-Opt. Instrum. Eng. **1431,** 122–135 (1991).
2. J. Fishkin and E. Gratton, "Propagation of photon-density waves in strongly scattering media containing an absorbing

semi-infinite plane bounded by a straight edge," J. Opt. Soc. Am. A **10,** 127–140 (1993).
3. M. A. O'Leary, D. A. Boas, B. Chance, and A. G. Yodh, "Refraction of diffuse photon density waves," Phys. Rev. Lett. **69,** 2658–2661 (1992).
4. B. J. Tromberg, L. O. Svaasand, T. T. Tsay, and R. C. Haskell, "Properties of photon density waves in multiple-scattering media," Appl. Opt. **32,** 607–616 (1993).
5. D. A. Boas, M. A. O'Leary, B. Chance, and A. G. Yodh, "Scattering of diffuse photon density waves by spherical inhomogeneities within turbid media: analytic solution and applications," Proc. Natl. Acad. Sci. USA **91,** 4887–4891 (1994).
6. A. Knuttel, J. M. Schmitt, and J. R. Knutson, "Spatial localization of absorbing bodies by interfering diffusive photon-density waves," Appl. Opt. **32,** 4, 381–389 (1993).
7. E. Gratton, W. W. Mantulin, M. J. vandeVen, J. B. Fishkin, M. B. Maris, and B. Chance, "A novel approach to laser tomography," Bioimaging **1,** 40–46 (1993).
8. M. A. O'Leary, D. A. Boas, B. Chance, and A. G. Yodh, "Imaging of inhomogeneous turbid media using diffuse photon density waves," in *Advances in Optical Imaging and Photon Migration,* Vol. 21 of 1994 OSA Proceedings (Optical Society of America, Washington, D.C., 1994), pp. 106–115.
9. R. Nossal, J. Kiefer, G. H. Weiss, R. Bonner, H. Taitelbaum, and S. Havlin, "Photon migration in layered media," Appl. Opt. **27,** 3382–3391 (1988).
10. A. Ishimaru, *Wave Propagation and Scattering in Random Media* (Academic, New York, 1978), Vol. 1, Chap. 9, pp. 175–190.
11. K. M. Case and P. F. Zweifel, *Linear Transport Theory* (Addison–Wesley, Reading, Mass., 1967), Chap. 8, pp. 194–231.
12. J. J. Duderstadt and L. J. Hamilton, *Nuclear Reactor Analysis* (Wiley, New York, 1976), Chap. 4, pp. 140–144.
13. S. Glasstone and A. Sesonske, *Nuclear Reactor Engineering,* 3rd ed. (Van Nostrand Reinhold, New York, 1981), Chap. 3, pp. 129–138.
14. J. A. Stratton, *Electromagnetic Theory* (McGraw-Hill, New York, 1949), Chap. 7, pp. 392–420.
15. W. C. Chew, *Waves and Fields in Inhomogeneous Media* (Van Nostrand Reinhold, New York, 1990), Chap. 3, pp. 184–199.
16. M. Abramowitz and I. A. Stegun, eds., *Handbook of Mathematical Functions* (Dover, New York, 1972), Chaps. 8 and 10, pp. 332–341, 437–454.
17. E. Gratton and J. Maier, "Frequency–domain measurements of photon migration in highly scattering media," in *Medical Optical Tomography: Functional Imaging and Monitoring,* G. J. Mueller, B. Chance, R. R. Alfano, S. R. Arridge, J. Beuthan, E. Gratton, U. Kaschke, B. R. Masters, S. Svanberg, P. van der Zee, eds., Vol. IS11 of the SPIE Institute Series (Society of Photo-Optical Instrumentation Engineers, Bellingham, Wash., 1993), pp. 534–544.
18. F. P. Bolin, L. E. Preuss, R. C. Taylor, and R. J. Ference, "Refractive index of some mammalian tissues using a fiber cladding method," Appl. Opt. **28,** 2297–2303 (1989).
19. R. L. Barbour, H. L. Graber, Y. Wang, J. Chang, and R. Aronson, "Perturbation approach for optical diffusing tomography using continuous-wave and time-resolved data," in *Medical Optical Tomography: Functional Imaging and Monitoring,* G. J. Mueller, B. Chance, R. R. Alfano, S. R. Arridge, J. Beuthan, E. Gratton, M. Kaschke, B. R. Masters, S. Svanberg, and P. van der Zee, eds., Vol. IS11 of the SPIE Institute Series (Society of Photo-Optical Instrumentation Engineers, Bellingham, Wash., 1993), pp. 87–120.
20. B. W. Pogue and M. S. Patterson, "Forward and inverse calculations for near-infrared imaging using a multigrid finite difference method," in *Advances in Optical Imaging and Photon Migration,* Vol. 21 of 1994 OSA Proceedings (Optical Society of America, Washington, D.C., 1994), pp. 176–180.
21. S. R. Arridge, "The forward and inverse problems in time-resolved infra-red imaging," in *Medical Optical Tomography: Functional Imaging and Monitoring,* G. J. Mueller, B. Chance, R. R. Alfano, S. R. Arridge, J. Beuthan, E. Gratton, M. Kaschke, B. R. Masters, S. Svanberg, and P. van der Zee, eds., Vol. IS11 of the SPIE Institute Series (Society of Photo-Optical Instrumentation Engineers, Bellingham, Wash., 1993), pp. 35–64.
22. J. R. Singer, F. A. Grunbaum, P. D. Kohn, and J. P. Zubelli, "Image reconstruction of the interior of bodies that diffuse radiation," Science **248,** 990–993 (1990).
23. J. A. Moon and J. Reintjes, "Image resolution by use of multiply scattered light," Opt. Lett. **19,** 521–523 (1994).
24. H. L. Graber, J. Chang, R. Aronson, and R. L. Barbour, "Perturbation model for imaging in dense scattering media: derivation and evaluation of imaging operators," in *Medical Optical Tomography: Functional Imaging and Monitoring,* G. J. Mueller, B. Chance, R. R. Alfano, S. R. Arridge, J. Beuthan, E. Gratton, M. Kaschke, B. R. Masters, S. Svanberg, and P. van der Zee, eds., Vol. IS11 of the SPIE Institute Series (Society of Photo-Optical Instrumentation Engineers, Bellingham, Wash., 1993), pp. 121–143.
25. J. Chang, H. L. Graber, P. C. Koo, R. Aronson, S. S. Barbour, and R. L. Barbour, "Progress toward optical mammography: imaging in dense scattering media using time-independent optical sources," in *Conference Record, 1994. IEEE Nuclear Space Symposium and Medical Imaging Conference* (Institute of Electrical and Electronics Engineers, New York, 1994), Vol. 3, pp. 1484–1488.